RSC Advances

A RNA Aptamer-Based Electrochemical Biosensor for Sensitive Detection of Malachite Green

Journal:	*RSC Advances*
Manuscript ID:	RA-ART-09-2014-009850.R1
Article Type:	Paper
Date Submitted by the Author:	20-Oct-2014

Complete List of Authors:	Wang, Hongzhi; University of Jinan, Key Laboratory of Chemical Sensing & Analysis in Universities of Shandong, School of Chemistry and Chemical Engineering Wang, Yu; University of Jinan, College of Biological Sciences and Technology Liu, Su; University of Jinan, College of Resources and Environment Yu, Jinghua; University of Jinan, Key Laboratory of Chemical Sensing & Analysis in Universities of Shandong, School of Chemistry and Chemical Engineering Xu, Wei; University of Jinan, Key Laboratory of Chemical Sensing & Analysis in Universities of Shandong, School of Chemistry and Chemical Engineering Guo, Yuna; University of Jinan, Key Laboratory of Chemical Sensing & Analysis in Universities of Shandong, School of Chemistry and Chemical Engineering Huang, Jiadong; University of Jinan,

A RNA Aptamer-Based Electrochemical Biosensor for Sensitive Detection of Malachite Green

Hongzhi Wang[a], Yu Wang[b], Su Liu[c], Jinghua Yu[a], Wei Xu[a], Yuna Guo[a], Jiadong Huang[a,b,*]

a *Key Laboratory of Chemical Sensing & Analysis in Universities of Shandong, School of Chemistry and Chemical Engineering, University of Jinan, Jinan 250022, P.R. China.*

b *College of Biological Sciences and Technology, University of Jinan, Jinan 250022, P.R. China*

c *College of Resources and Environment, University of Jinan, Jinan 250022, P.R. China*

[*] Corresponding author. Tel.: +86-531-89736122; Fax: +86-531- 82769122.

E-mail: chm_huangjd@ujn.edu.cn.

Abstract

A RNA aptamer-based electrochemical biosensing strategy has been developed for sensitive and selective detection of malachite green (MG). This biosensor is fabricated by the self-assembly of thiolated MG aptamer (MGA) on AuNPs/graphene-chitosan nanocomposites modified glass carbon electrode. In addition, a short alkanethiol is further assembled on AuNPs surface to generate uniform packing and reduce nonspecific adsorption. When the modified electrode is incubated in the presence of MG, MGA combines specifically with MG, which causes the horseradish peroxidase (HRP)-labelled MG antibody close to the electrode surfaces. As a result, MG detection is realized by outputting a redox current from electro-reduction of hydrogen peroxide reaction catalyzed by HRP. Differential pulse voltammetry (DPV) is performed to record the signal responses. The results reveal the biosensor displays very low detection limit as low as 16.3 pg mL^{-1} and a wide linear range from 1×10^{-4} to 10 μg mL^{-1} of MG. Hence, this proposed RNA aptamer-based electrochemical strategy may offer a simple, rapid, cost-effective, highly selective and sensitive method for the quantification of MG.

Keywords: malachite green; RNA aptamer; electrochemical; Au nanoparticles; rGO-CS nanocomposites

1. Introduction

Malachite green (MG), a cationic triphenylmethane dye, has been widely used in commercial aquaculture [1]. MG is especially active against the *Saprolegnia* fungus, which infects fish and fish eggs [2]. It is also used to resist parasitic and bacterial infections, especially in the treatment of farmed freshwater fish [3]. However, MG is reported to be toxic to humans and animals even at trace concentration because of its adverse effects on the immune and reproductive systems, infertility and respiratory ailments [4, 5]. For this reason, the European Union has set a minimum required performance limit for MG at a level of 2 μg kg^{-1} [6]. Therefore, screening and confirmatory methods must have the ability of detecting MG at concentrations at or below 2 μg kg^{-1}.

Current available methods for MG assay mainly include high-performance liquid chromatography assay [7], spectrophotometric assay [8] and enzyme-linked immunosorbent assay [9]. Although these approaches are quite sensitive and accurate, they may suffer from some shortcomings such as complicated operation, expensive instrumentations and expert technical skill. Therefore, the development of simple, rapid and cost-effective methods for the sensitive and specific detection of MG still remains a grand challenge.

Generally, electrochemical detection can be readily miniaturized and automated with low cost, high detection speed, and minimal sample consumption. Moreover, this platform does not demand high-voltage power supplies, light sources or other sophisticated equipment. In view of these advantages, electrochemically based bio-sensing strategies seem to be suitable for practical applications. As expected, the activity of the immobilized bio-molecules is a key factor for developing biosensors with excellent performance, which demands highly dense immobilization of bio-molecules, proper bio-molecule orientation to permit specific interactions, and long-term stability of attached bio-molecules. Aptamer, a short, synthetic and single-stranded RNA or DNA molecule can be generally prepared using an *in vitro* method known as systematic evolution of ligands by exponential enrichment (SELEX) [10]. Aptamers have been recognized as an excellent choice for immobilized

bio-molecules. They can bind specially to target molecules with high affinity, which range from small molecules to macro-molecules, for example, organic dyes [11], metal ions [12], proteins [13] and even whole cells [14]. Up to now, aptamers have been used as a versatile and useful molecule recognition tool due to their easy synthesis, facile modification and high chemical stability [15].

To achieve highly dense immobilization of bio-molecules and improve the charge-transport property of electrode, a wide variety of nanomaterials have been used as ideal components in constructing electrochemically based biosensors, such as metal nanoparticles [16], graphene [17], carbon nanotubes [18], conducting polymer [19], chitosan (CS) [20] and so on. Among various metal nanoparticles, Au nanoparticles (AuNPs) have attracted much attention because of their rapid and easy synthesis, narrow size distribution, and efficient surface modification by thiols or other bioligands [21]. Reduced graphene oxide (rGO), a new class of two-dimensional sheet of carbon nanostructure with large specific surface area, relatively high electrical conductivity and excellent bio-compatibility, has been widely applied to electrode surface modification [22]. CS, which has desirable film-forming ability, has been used as an immobilization matrix to increase the solubility and dispersion of chemicals and nanomaterials [23].

Herein, a RNA aptamer-based electrochemical biosensing strategy has been reported for sensitive and selective detection of MG. By modification of RNA aptamer with a terminal thiolated RNA aptamer can be readily immobilized on AuNPs surfaces and form a self-assembled monolayer, which leads to orientational and highly dense immobilization of aptamer. Additionally, a short alkanethiol [24] is introduced for the surface modification of AuNPs to generate uniform packing and reduce nonspecific adsorption. This biosensor has the advantages of high sensitivity, specificity, wide linear range, rapid, convenient, and low cost detection with simple operation. Thus, the proposed RNA aptamer-based electrochemical biosensor may contribute a new platform for the quantification of MG.

2. Experimental Section

2.1 Reagents and materials

The horseradish peroxidase-labelled MG antibody (HRP-labelled MG Ab) was purchased from Beijing Kwinbon Biotechnology Co. Ltd (Beijing, China). MG, gold (III) chloride trihydrate ($HAuCl_4 \cdot 3H_2O$), chloramphenicol, and bovine serum albumin (BSA) were obtained from Sigma Aldrich (St. Louis, MO, USA). MG ELISA kit was purchased from Longrun Biological Technology Co. Ltd (Beijing, China). Leucomalachite green (LMG), hydroquinone (HQ), diethy pyrocarbonate (DEPC) and H_2O_2 were obtained from Aladdin Chemistry Co., Ltd. (China). CS was purchased from Sangon Biotech Co., Ltd. (Shanghai, China). All other chemicals were of analytical grade and obtained from Sinopharm Chemical Reagent Co. Ltd (Beijing, China). All solutions were prepared using ultrapure water with an electric resistance >18.25 MΩ, which was obtained through a Millipore Milli-Q water purification system (Billerica, MA, USA). Oligonucleotides used in this work were synthesized by Shanghai Sangon Biotechnology Co. Ltd. (Shanghai, China). The sequence of the thiolated MG aptamer (thiolated MGA) is 5'-SH-GGAUCCCGACUGGCGAGAGCCAGGUAACGAAUGGAUCC-3'.

2.2 Apparatus

Scanning electron micrographs (SEMs) were obtained using a field emission emission scanning electron microscope (ZEISS, Germany). Fourier transform infrared (FT-IR) spectra and un-visible spectra were recorded using a Spectrum One FT-IR Apparatus (Perkin Elmer, USA) and a Lambda 35 Spectrometer (PerkinElmer, USA) in the wavelength range from 200 to 800 nm, respectively.

Cyclic voltammetry (CV) measurements, electrochemical impedance spectroscopy (EIS) and differential pulse voltammetry (DPV) measurements were carried out using a CHI 660D electrochemical workstation (Shanghai CH Instruments, China). All experiments were performed using a conventional three-electrode system consisting of a Ag/AgCl reference electrode, a platinum wire auxiliary electrode and a modified glassy carbon working electrode.

2.3 Synthesis of rGO-CS nanocomposites

Graphite oxide (GO) was prepared by a modified Hummers method [25]. In our

work, 1 g graphite powder was added to 0.5 g $NaNO_3$ and 23 mL H_2SO_4 (98%), and the mixture was stirred for 30 min in an ice-salt bath at 0 ℃. Then, 3 g $KMnO_4$ was slowly added into the solution at 20 ℃. After being stirred for 1 h, the solution temperature was raised gradually to 35 ℃ in a water bath and remained for more than 30 min. Then 100 mL deionized water was added into the solution and kept stirring for another 20 min. After sufficiently stirring the mixture, 50 mL H_2O_2 (30 %) was added into the mixture until the color of the suspension changed from brown to brilliant yellow. The solution was filtered and washed three times with deionized water. Then the obtained products were dried at 60 ℃ for 24 h. Next, the prepared GO (20 mg) was dispersed into 20 mL of deionized water and sonicated for 8 h. Then 0.5 mL of poly (4-styrenesulfonic acid) and hydrazine were added into the resulting dispersion, which was continuously stirred at 90 ℃ for 24 h. After cooling to room temperature (RT), the mixture was washed for three times using deionized water and then dried at 60 ℃. Thirdly, 50 mg CS was dissolved into 10 mL of 1.0 % (v/v) acetic acid solution and then the mixture was stirred for 2 h at RT until it was completely dispersed. The rGO-CS composites were synthesized according to a previously reported protocol [26]. Briefly, 1 mg rGO was added to 1 mL of CS, and the mixture was sufficiently stirred to achieve a homogeneous solution.

2.4 Preparation of Au nanoparticles

The AuNPs were prepared using a trisodium citrate reduction method according to a previous reported method with slight modifications as follows [27]. Briefly, 2 mL of 1 % trisodium citrate solution was added rapidly under vigorous stirring in 100 mL of 0.01 % boiling $HAuCl_4$ solution. Within several minutes, the solution color changed from yellowish to wine red. The solution was heated under reflux for another 20 min to ensure complete reduction, and it was then slowly cooled to RT and stored at 4 ºC before use.

2.5 The fabrication process of the biosensor

The glass carbon electrode (GCE) was polished sequentially with 0.3 and 0.05 μm alumina powder, followed by ultrasonic cleaning in ethanol and doubly distilled water. The cleaned GCE displayed a mirror like surface. Then, the electrodes were

washed with deionized water and dried for further use. Typically, 10 μL of rGO-CS nanocomposite solution was applied to the GCE. After incubating at RT for 4 h, 10 μL of AuNP solution was placed on the modified electrode before the electrode was dried at RT. The modified electrode was washed three times using 10 mM phosphate buffered saline (PBS) and then air dried.

Next, 10 μL of a thiolated MGA (50 μM) was added on an AuNPs/rGO-CS/GCE before the electrode was incubated for 16 h at 4 ℃. After that, the electrode was rinsed in DEPC-treated water for 10 min to remove the nonspecific adsorption. Then, 10 μL of 6-mercapto-1-hexanol (100 μM) was added on the modified electrode and incubated for 2 h at RT. After that, the modified electrode was thoroughly rinsed with 10 mM PBS to remove the non-specific binding and stored for further use at 4 ℃.

2.6 Electrochemical measurements

Electrochemical measurements were carried out to characterize the modified electrode. CV measurements were performed over a potential range from -0.2 V to +0.6 V at a scan rate of 50 mV s^{-1} in 5 mM $K_3[Fe(CN)_6]$ containing 0.2 M KCl , while DPV was carried out in PBS (pH 7.4) containing 1 mM HQ and 10 mM H_2O_2. EIS measurements were performed from 0.1 to 10^5 Hz in PBS (pH 7.4) containing 0.2 M KCl and 5.0 mM $K_3[Fe(CN)_6]$.

3. Results and Discussion

3.1 Scheme of the electrochemical biosensor

(Scheme 1)

Scheme 1 shows the structure for the proposed electrochemical biosensor based on RNA aptamer. This biosensor was fabricated by the self-assembly of thiolated MGA on the AuNPs/rGO-CS nanocomposites modified GCE, which as electrode materials could significantly improve charge-transport property and loading capacity of the biomolecules. To reduce non-specific adsorption, the short alkanethiol, 6-mercapto-1-hexanol, was self-assembled on the AuNPs by exploiting the Au-S covalent interaction. By incubating in MG, MGA on the electrode surface would specifically interact with MG, leaving a different epitode on MG to interact with HRP-labelled MG Ab. In this way, HRP would catalyze the reaction between H_2O_2

and HQ to yield BQ, which was easily restored back to HQ. The reduction of BQ was then used to quantitatively related to MG.

3.2 Electrochemical behaviors

Fig. 1 depicts typical DPV responses of the biosensor in the assay of MG. In the absence of target MG, a relatively weak DPV peak current was obtained, implying almost no HRP-labelled MG Ab was fixed on the surfaces of modified electrode (curve a). In contrast, it was observed that a significantly increased peak current appeared after the modified electrode incubated with 10 μg mL^{-1} MG, which was attributed that HRP-labelled antibody combined specifically with MG and catalyzed the oxidation of HQ (curve b). These data indicated that the enhanced DPV signal was induced by specific immunological recognition events rather than non-specific interactions. To highlight the electronic conductivity of AuNPs/rGO-CS nanocomposites, other two types of biosensors, MGA/rGO-CS/GCE and MGA/AuNPs/GCE were fabricated, respectively. It was found that the biosensor using AuNPs/rGO-CS nanocomposites as electrode materials exhibited remarkably improved excellent electron transfer efficiency than that using either AuNPs (curve c) or rGO-CS (curve d). These findings gave clear evidence that AuNPs/rGO-CS composites significantly facilitated the electron transfer rate between the modified electrode and the working solution and improved the performance in electrochemical signal transduction.

(Fig. 1)

To promote charge-transport efficiency and improve biosensor performance, AuNPs/rGO-CS nanocomposites were immobilized on the GCE surface, which as electrodes materials could remarkably enhance electron transfer rate between the electrodes and the electrolyte solution. CV measurements were performed to probe the electron transfer efficiency of the modified electrodes. The results were shown in Fig. 2. With the bare GCE, a pair of well-defined redox peaks appeared at 0.17 mV and 0.26 mV, a typical redox peak range of $K_3[Fe(CN)_6]$ (curve a). With the electrode modified with rGO, a corresponding peak current was observed, which was ~100% stronger than that of curve a (curve b). The reason might be that rGO often suffered

from irreversible cohesion and formed agglomerates, which could hinder electrolyte penetration into layers and adversely affected the electron transfer efficiency [28]. In contrast, an obviously increased CV signal (~270% stronger than that of curve a) was obtained after immobilizing rGO-CS nanocomposites on the electrode surface (curve c). This was ascribed to the excellent film-forming ability of chitosan, which could increase the dispersibility of rGO and improve electron transfer efficiency. With the electrode decorated with AuNPs/rGO-CS nanocomposites, there was a very strong peak current in the CV curves (~460% stronger than that of curve a), indicating the excellent electrical conductivity of the rGO-CS nanocomposite (curve d). After MGA and alkanethiol assembling on the surfaces of modified electrode, it was observed that a dramatically weaker current signal appeared, which suggested MGA-alkanethiol mixed monolayers formed on the electrode could block the electron transfer between the electrode and the electrolyte solution (curve e). When the modified electrode incubated with 10 μg mL^{-1} MG solution, a mildly increased peak current was achieved (~30 % stronger than that of curve e), which was attributed that MG was a redox polymer and its redox reaction possibly resulted from its quinoid structure [29] (curve f). After incubating with HRP-labelled MG Ab solution, we observed a significantly decreased peak current signalappeared in the CV curves (50% weaker than that of curve f), implying the electron transport was hindered due to the isolated biomolecules (curve g). These observations confirmed that the AuNPs/rGO-CS nanocomposites played a crucial role in the electrochemical transduction and the sensing interface for MG was successfully constructed.

(Fig. 2)

Impedance spectroscopy is an effective method for studying the features of surface-modified electrodes. EIS measurements were performed to investigate the electrode modified by different procedures. Fig. 3 depicted Nyquist plots obtained in the fabrication process of the modified electrodes. It was found that the impedance plot for rGO-CS/GCE (curve a) or AuNPs/rGO-CS/GCE (curve b) displayed an almost straight line. This revealed that the electron transfer was very easy due to the excellent charge-transport efficiency of electrodes materials. After immobilizing

MGA on the surfaces of AuNPs/rGO-CS/GCE, a significantly increased faraday impedance was observed, implying successful assembly of MGA on the electrode surface (curve c). After incubation the modified electrode with 10 μg mL^{-1} MG solution, there was a little decrease of the semicircle diameter (curve d). The reason for this phenomenon might be attributed that MG is a redox polymer and its redox reaction possibly results from its quinoid structure. After incubating with HRP-labelled MG Ab solution, the modified electrode gave a very large impedance, indicating the isolating behavior of biomacromolecules (curve e). On the basis of these results, it was reasonably concluded that the fabrication of the sensing interface for MG was successfully achieved.

(Fig. 3)

3.3 Characterization of rGO-CS nanocomposites and Au nanoparticles

Scanning electron microscopy was employed to investigate the morphology and micro-structure of the as-prepared nanocomposites, as shown in Fig. 4A. With the electrode modified by rGO-CS nanocomposites, it was observed that the nanocomposites displayed the typically flake-like with slightly crumpled and wrinkled edge (Fig. 4A (a)) [30]. With the electrode modified by AuNPs/rGO-CS nanocomposites, we observed from the micro-graph that AuNPs were uniformly deposited on the rGO-CS flakes. This illustrated AuNPs was immobilized on the electrode surface through electrostatic interaction between AuNPs and rGO.

FT-IR characterization was performed to inspect the as-prepared pure GO and rGO. Fig. 4B showed the FTIR spectra of pure GO and rGO, respectively. From the spectrum of GO (curve a), the main absorption band at 3400 cm^{-1} is assigned to the O-H group stretching vibrations. The absorption peaks at 1730 cm^{-1} and 1625 cm^{-1} were assigned to C=O stretching of carboxyl and/or carbonyl moiety functional groups. The spectra also show other absorption peaks at 1228 cm^{-1} and 1044 cm^{-1}, which correspond to the C-O stretching vibrations. Compared to the above bands of GO, there were no obvious absorption peak for pure rGO except 1630 cm^{-1} and 3440 cm^{-1}, which might be attributed to some C=O residues at the edges of the rGO (curve b). This suggested the hydroxy, carboxyl and epoxy groups of GO were successfully

reduced. Additionally, uv-vis spectral analysis was performed to verify the formation of AuNPs. As shown in Fig. 4C, no absorption peak was obtained in the presence of $HAuCl_4$ solution (curve a). In contrast, an obvious absorption peak appeared at 520 nm, typical for individual AuNPs of ~13 nm [31].

(Fig. 4)

3.4 Optimization of experimental conditions

The immobilization of the MGA was a crucial step in the fabrication of biosensor. Hence, the effect of the incubation time of MGA on electrode was investigated. A series of AuNPs/rGO-CS/GCE were incubated with 10 μM MGA solution for 2, 4, 8, 16, and 24 h at 4℃, respectively. As shown in Fig. 5A, with the increase of incubation time from 2 h to 16 h, the biosensors showed an increasing DPV response until the incubation time of 16 h when the signal nearly reached equilibrium. Therefore, the incubation time of 16 h was chosen as the optimal incubation time.

The concentration of the HRP-labelled MG Ab on the modified electrodes is an important factor that affected the DPV signal of the biosensor. A series of MG/MGA/AuNPs/rGO-CS/GCE were incubated with different concentrations of HRP-labelled MG Ab solution (0.1, 1, 10, 100 and 1000 μM) for 60 min at RT. As shown in Fig. 5B, the DPV signals increased with the increase of HRP-labelled MG Ab concentration and reached equilibrium when the concentration was 100 μM. Thus, the concentration of 100 μM was chosen as the optimal concentration.

The effect of the incubation time of the HRP-labelled MG Ab on the modified electrodes was also investigated. A series of MG/MGA/AuNPs/rGO-CS/GCE were incubated with 100 μM HRP-labelled MG Ab solution for 20, 40, 60, 90, and 120 min at RT, respectively. As shown in Fig. 5C, with the increase of incubation time from 20 min to 60 min, the biosensors showed an increasing DPV response until the incubation time of 60 min when the signal nearly reached equilibrium. Therefore, the incubation time of 60 min was chosen as the optimal incubation time.

The pH of working solution also had a very important influence on the performance of the biosensor. A series of HRP-labelled MG Ab /MG/MGA/AuNPs/rGO-CS/GCE were immersed to working solution with different

pH. As shown in Fig. 5D, the current responses significantly increased with pH from 6 to 7, but decreased above 7. Hence, we chose 7 as the optimal pH of working solution.

(Fig. 5)

3.7 Calibration curve of biosensor

Fig. 6A depicts typical DPV responses of the biosensor to MG of varying concentrations. We observed dynamically increased DPV peaks in response to MG of increasing concentrations within the range from 1×10^{-4} μg mL^{-1} to 10 μg mL^{-1}. By fitting the data in the concentration range below 10 μg mL^{-1} to a linear model I = 26.527 + 1.412 × logC (I (10^{-6} A) is the peak current intensity and C (μg mL^{-1}) is the concentration of MG), the LOD of the proposed method was calculated to be 16.3 pg mL^{-1} in terms of the rule of 3 times standard deviation over the blank response. The LOD was lower than that of previous research [32]. These results demonstrated that the biosensing strategy could be used for quantitative analysis of MG targets.

(Fig. 6)

3.8 The selectivity, reproducibility, and stability of the biosensor

To confirm the reliability of the fabricated biosensor, the binding specificity of the biosensor for 10 μg mL^{-1} MG and other structural analogs (100 μg mL^{-1}), such as chloramphenicol and LMG, was also evaluated. As shown in Fig. 7, the current variation in the presence of the interfering substances was all less than 4%. These results indicated that the proposed biosensor exhibited selectivity towards MG.

(Fig. 7)

To investigate the reproducibility of the biosensor, five electrodes with the same assembly step were utilized to detect 0.1 μg mL^{-1} MG, respectively. The current responses showed a relative standard deviation (RSD) of 3.5% for five independent measurements. This suggested that the preparation of the biosensor presented very good reproducibility.

Besides, we also investigated the stability of the biosensor. Five electrodes were fabricated independently under the same conditions and stored at 4 ℃ for 2 weeks. Then these electrodes were used to detect 0.1 μg mL^{-1} MG. The results showed that

about 92 % of its initial response of the biosensor for MG remained, which indicated this biosensor had very desirable stability.

3.9 Real samples analysis

The feasibility of the proposed biosensor for quantitative assay of MG in fishery water was also investigated. Different concentrations of MG in fishery water by standard addition methods were used to inspect the recovery. Tab. 1 depicted the results in the assays for the synthetic samples by using our method and the enzyme-linked immunosorbent assay (ELISA) method. It was observed that the results obtained via our method were consisted with those of ELISA method, and the discrepancies between two methods were all smaller than 10.0%. Besides, the recovery of the proposed method was in the range of 94.6%-105.7%. These data clearly demonstrated the potential of our method for applications in complicated samples.

(Tab. 1.)

4. Conclusion

In this paper, we developed a RNA aptamer-based electrochemical biosensing strategy for sensitive and selective detection of MG. This biosensor was fabricated by the self-assembly of thiolated MGA on an AuNPs/rGO-CS nanocomposite modified GCE. Moreover, a short alkanethiol was used for surface modification of electrode to promote uniform packing and reduce nonspecific adsorption. The results showed the biosensor displayed a widened linear range from 1×10^{-4} to 10 μg mL^{-1} and an improved detection limit down to 16.3 pg mL^{-1} for detecting MG. Additionally, our method offers simplified operations and shortened analysis time with no need of multiple washing steps and large amount of reagent consuming. Thus, the proposed biosensor has the advantages in its simplicity, rapidness, and low cost detection compared to traditional methods, such as high-performance liquid chromatography assay [7], spectrophotometric assay [8] and enzyme-linked immunosorbent assay [9]. Thus, the proposed RNA aptamer-based electrochemical biosensor may contribute a new platform to the quantification of MG.

Acknowledgements

This work was supported by the National Natural Science Foundation of the People's Republic of China (no. 31171700 and 31101296), the National High Technology Research and Development Program of China (National 863 Program of China) (no. 2012AA101604), the Natural Science Foundation of Shandong Province (no. ZR2010DQ025) and the Shandong Province Higher Educational Science and Technology Program (no. J10LB14)

References

[1] A.N. Kagalkar, M.U. Jadhav, V.A. Bapat, S.P. Govindwar, *Bioresour. Technol*., 2011, **102**, 10312-10318.

[2] V. Chaturvedi, K. Bhange, R. Bhatt, P. Verma, *J. Environ. Chem. Eng.*, 2013, 1, 1205–1213.

[3] M.A. Pierrard, P. Kestemont, E. Delaive, M. Dieub, M. Raes, F. Silvestre, *Aquat. Toxicol.*, 2012, **114**, 142– 152.

[4] F. Ding, X.N. Li, J.X. Diao, Y. Sun, L. Zhang, L. Ma, X.L. Yang, L. Zhang, Y. Sun, *Ecotoxicol. Environ. Saf.*, 2012, **78**, 41–49.

[5] R. Ahmad, R. Kumar, *J. Environ. Manage.*, 2010, **91**, 1032–1038.

[7] K. Mitrowska, A. Posyniak, *J. Zmudzki, J. Chromatogr. A*, 2005, **1089**, 187–192.

[8] C. Nebot, A. Iglesias, R. Barreiro, J.M. Miranda, B.Vázquez, C. M. Franco, A. Cepeda, *Food Control*, 2013, **31**, 102-107.

[9] N. Biland zi, I. Varenina, B.S. Kolanovi, D. Orai, S. Zrn ci, *Food Control*, 2012, **26**, 393-396.

[10] T.L. Huey, X. Hang, L. Yi, *Acc. Chem. Res.*, 2014, **47**, 1881-1890.

[11] Z.Y. Lin, H.M. Huang, Y.X. Xu, X.Y. Gao, B. Qiu, X. Chen, G.N. Chen, *Talanta*, 2013, **103**, 371–374.

[12] X. Zhu, Y.S. Zhang, W.Q. Yang, Q.D. Liu, Z.Y. Lin, B. Qiu, G.N. *Chen, Anal. Chim. Acta.*, 2011, **684**, 121–125.

[13] Y.F. Li, J.C. Bao, M. Han, Z.H. Dai, H.S. Wang, *Biosens. Bioelectron*, 2011, **26**, 3531–3535.

[14] J. Ashley, S.F.Y. Li, *Biosens. Bioelectron*, 2013, **48**, 126–131.

[15] L. Hao, X.B. Zhang, Y.F. Lv, *Acc. Chem. Res.*, 2014, **47**, 1891-1901.

[16] H.H. Huang, E. Ruckenstein, *J. Phys. Chem. B.*, 2013, **117**, 6318-6322.

[17] N. Li, X.M. Zhang, Q. Song, R.G. Su, Q. Zhang, T. Kong, L.W. Liu, G. Jin, M.L. Tang, G.S. Cheng, *Biomaterials.*, 2011, **32**, 9374-9382.

[18] L. Wang, A. Ambrosi, M. Pumera, *Anal. Chem.*, 2013, **85**, 6195-6197.

[19] A.Q. Contractor, V.A. Juvekar, *Anal. Chem.*, 2014, **86**, 6323-6330.

[20] A. Sivanesan, G. Kalaivani, A. Fischer, K. Stiba, S. Leimkuhler, L.M. Weidinger, *Anal. Chem.*, 2012, **84**, 5759-5764.

[21] L. A.nnika, P.B. Yu, S. Ulrich, *Nanoscale*, 2013, **5**, 6224-6242.

[22] T. Panagiotis, F. Thomas, S.P. Carbon, *Carbon*, 2014, **57**, 5-42.

[23] M. Videira, A. Arranja, D. Rafael, *Nanomedicine*, 2014, **10**, 689-702.

[24] Y.Y. Yeneneh, J.C. Kshitij, T. Mesfin, *Nanoscale*, 2014, **6**, 3496-3502.

[25] B**.**W. Hummersjr, R. Offeman, *J. Am. Chem. Soc.*, 1957, **25**, 1339.

[26] W. Xue, L. Hui, W. Min, G.S. Li, Z. Yan, W.Q. Jiang, H.P. Gang, F.Y. Zhi, *Chin J Anal Chem.*, 2013, **41**, 1232–1237.

[27] M.H. Xiang, X. Xu, F. Liu, N. Li, K.A. Li, *J. Phys. Chem. B.*, 2009, **113**, 2734–2738.

[28] C. Zhang, Z. Zhang, G. Li, *J. Chromatogr. A*, 2014, **1346**, 8-15.

[29] Q.J. Wan, X.X. Wang , X. Wang, N.J. Yang, *Polymer*, 2006, **47**, 7684-7692.

[30] H.S. Yin, Q. Ma, Y.L. Zhou, S.Y. Ai, L.S. Zhu, *Electrochim. Acta.*, 2010, **55**, 7102-7108.

[31] S. Patil, S. Datar, N. Rekha, S.K. Asha, C.V. Dharmadhikari, *Nanoscale*, 2013, **5**, 4404-4411.

[32] A.A. Fallah, A. Barani, *Food Control*, 2014, **40**, 100-105.

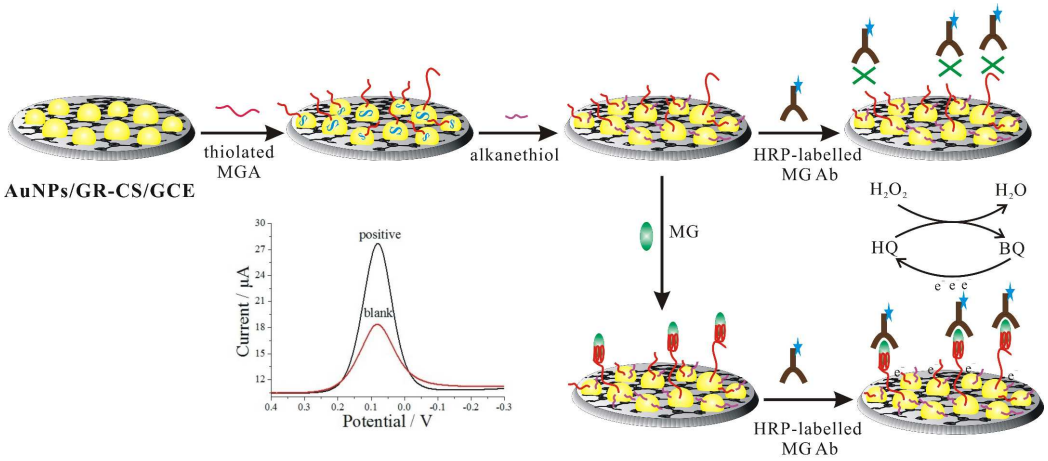

Scheme 1. Schematic illustration of the RNA aptamer-based electrochemical biosensor.

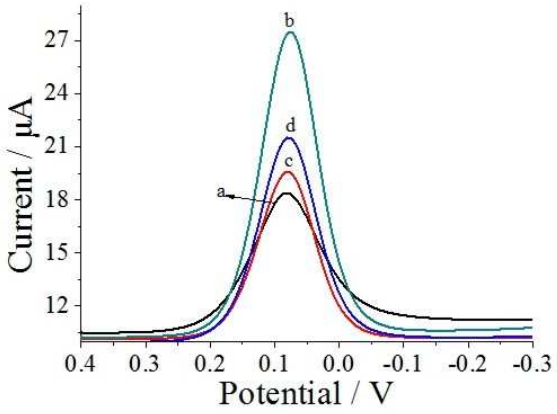

434

435 Fig. 1. (a) Typical DPVs of the immunosensors using AuNPs/rGO-CS nanocomposites as
436 electrode materials incubated in the absence of MG. (b-d) Typical DPVs of the immunosensors
437 using AuNPs/rGO-CS nanocomposites (b), AuNPs (c) and rGO-CS nanocomposites (d) as
438 electrode materials incubated in the presence of 10 μg mL^{-1} MG. DPV measurements were
439 performed in 0.01 M PBS (pH 7.4) containing 0.2 M KCl, 1 mM HQ, and 10 mM H_2O_2.

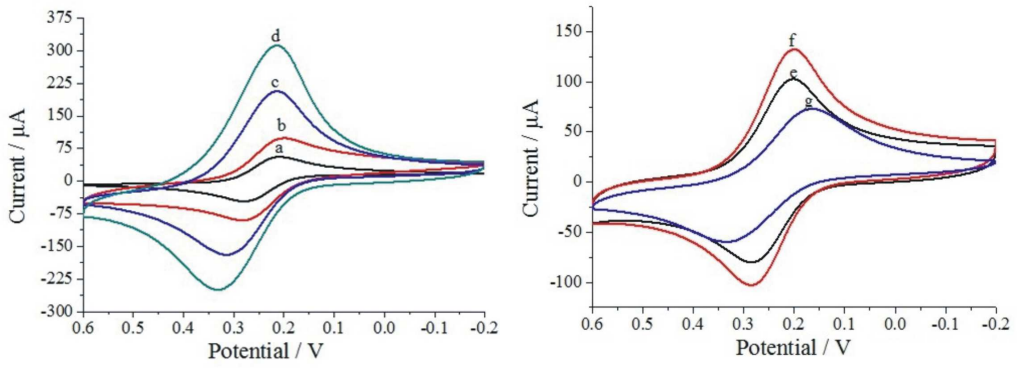

440

441 Fig. 2. CVs obtained for the bare GCE (a), rGO/GCE (b), rGO-CS/GCE (c), AuNPs/rGO-CS/GCE

442 (d), CVs obtained for the bare MGA/AuNPs/rGO-CS/GCE (e), MG/MGA/AuNPs/rGO-CS/GCE

443 (f), MG Ab/MG/MGA/AuNPs/rGO-CS/GCE (g). Measurements were performed in PBS

444 containing 0.2 M KCl and 5.0 mM $K_3[Fe(CN)_6]$.

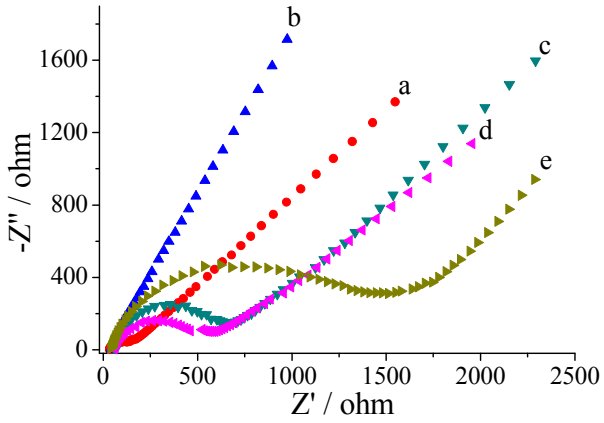

445

446 Fig. 3. EIS obtained for rGO-CS/GCE (a), AuNPs/rGO-CS/GCE (b), MGA/AuNPs/rGO-CS/GCE

447 (c), MG/MGA/AuNPs/rGO-CS/GCE (d), MG Ab/MG/MGA/AuNPs/rGO-CS/GCE (e).

448 Measurements were performed from 0.1 to 10^5 Hz in PBS containing 0.2 M KCl and 5.0 mM

449 $K_3[Fe(CN)_6]$.

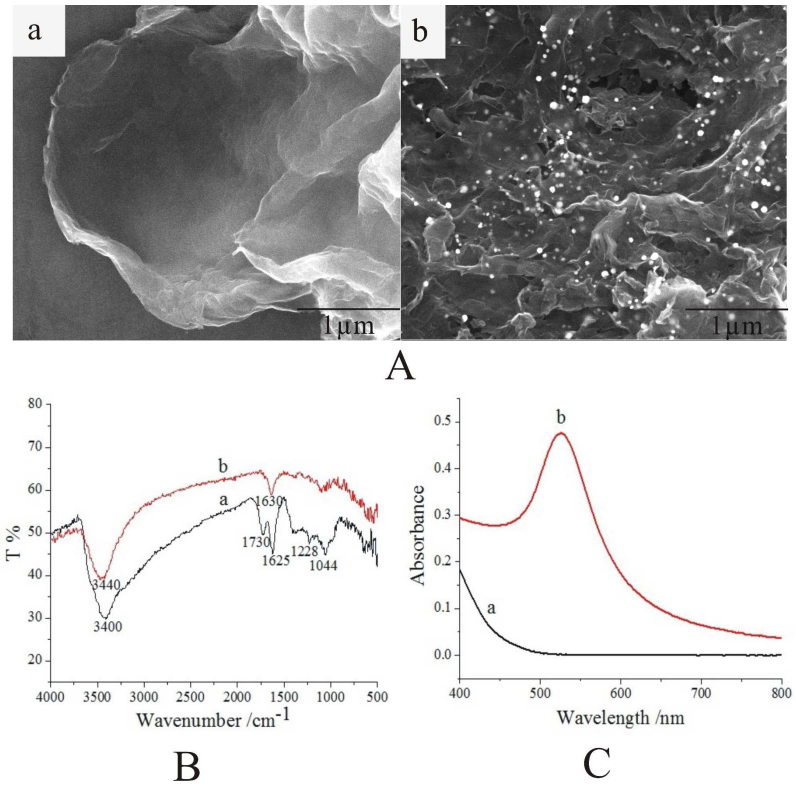

Fig. 4. (A) SEM images of rGO-CS nanocomposites (a) and AuNPs/rGO-CS nanocomposites (b) deposited on GCE. (B) FT-IR spectrum obtained for pure GO (a) and rGO (b). (C) UV-vis absorption spectra obtained for 3 µM $HAuCl_4$ solution (a) and 1.8 nM AuNPs solution (b).

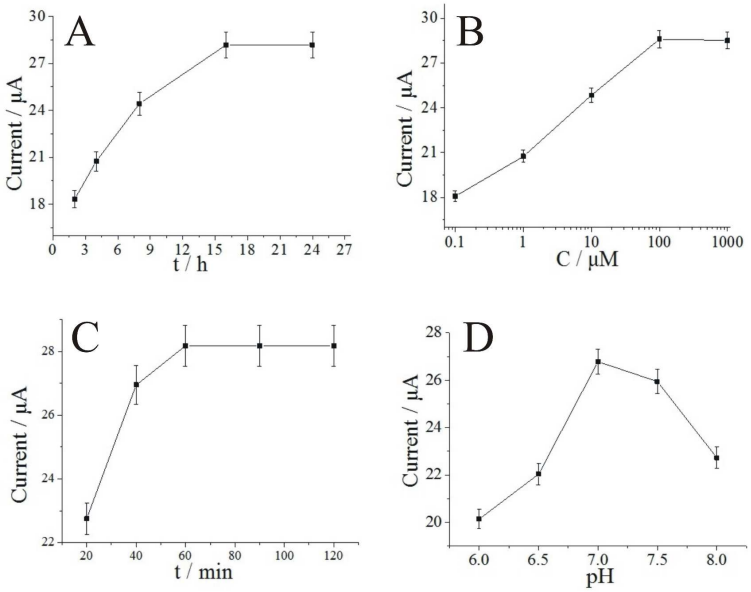

Fig. 5. (A) Effect of the incubation time of the MGA on the DPV peak current of biosensor. (B) Effect of the concentration of HRP-labelled MG Ab on the DPV peak current of biosensor. (C) Effect of the incubation time of HRP-labelled MG Ab on the DPV peak current of biosensor. The concentration of MG is 10 μg mL^{-1}. (D) Effect of pH of the working buffer solution on the DPV peak current of biosensor.

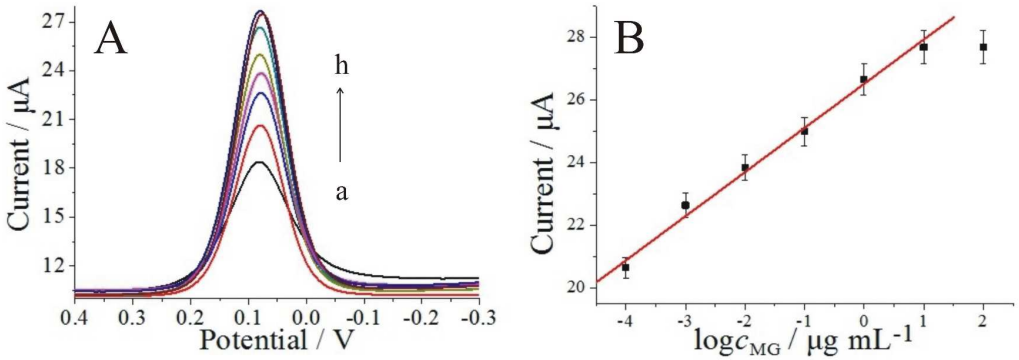

Fig. 6. (A) Typical DPV responses of the biosensor to different concentrations of MG (from curve a to h: 0, 1×10^{-4}, 1×10^{-3}, 1×10^{-2}, 1×10^{-1}, 1, 10, 100 μg mL^{-1}). (B) The calibration curve of current response versus the logarithm of MG with various concentrations.

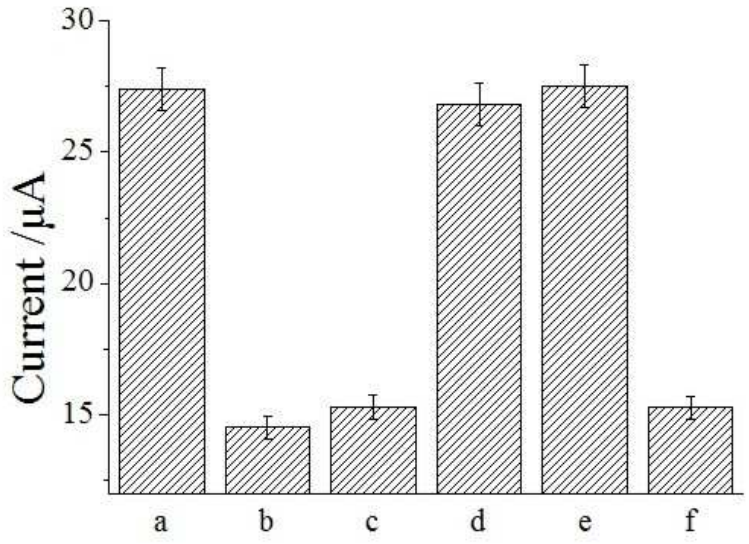

475

476 Fig. 7. DPV currrent responses of the biosensor to MG (10 μg mL^{-1}) (a), chloramphenicol (100 μg
477 mL^{-1}) (b), LMG (100 μg mL^{-1}) (c), MG (10 μg mL^{-1}) and chloramphenicol (100 μg mL^{-1}) (d), MG
478 (10 μg mL^{-1}) and LMG (100 μg mL^{-1}) (e), chloramphenicol (100 μg mL^{-1}) and LMG (100 μg
479 mL^{-1}) (f). Error bars are standard deviations across three repetitive experiments.

480 Tab. 1. MG analysis in synthetic samples.

MG in fishery water ($\mu g\ mL^{-1}$)	Our method ($\mu g\ mL^{-1}$)	Recovery (%)	ELISA method ($\mu g\ mL^{-1}$)
1.000×10^{-3}	$(0.946\pm0.047)\times10^{-3}$	94.6	1.035×10^{-3}
1.000×10^{-2}	$(1.057\pm0.053)\times10^{-2}$	105.7	0.961×10^{-2}
1.000×10^{-1}	$(1.034\pm0.052)\times10^{-1}$	103.4	1.029×10^{-1}
1.000	0.983±0.049	98.3	1.037

481

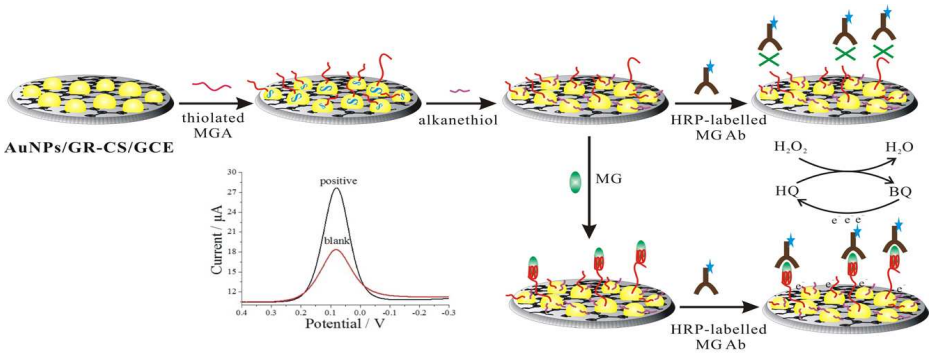
AuNPs/GR-CS/GCE
thiolated MGA
alkanethiol
HRP-labelled MG Ab
MG
positive
blank
Current / μA
Potential / V
H_2O_2
H_2O
HQ
BQ
e e e
HRP-labelled MG Ab

Title Text

A RNA Aptamer-Based Electrochemical Biosensor for Sensitive Detection of Malachite Green

*Hongzhi Wang, Yu Wang, Su Liu, Jinghua Yu, Wei Xu, Yuna Guo, Jiadong Huang**

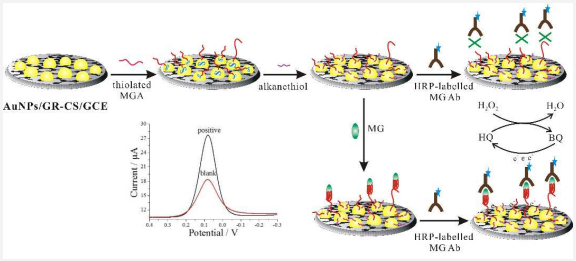

A RNA aptamer-based electrochemical biosensing strategy has been developed for sensitive and selective detection of malachite green.